Monte Carlo approach to island formation during thermal treatment of thin films

F. Lallet, R. Bachelet, A. Dauger, and N. Olivi-Tran
Laboratoire de Sciences des Procédés Céramiques et Traitements de Surface, UMR-CNRS 6638, Ecole Nationale Supérieure de Céramiques Industrielles, 47 Avenue Albert Thomas, 87065 Limoges Cedex, France
(Received 12 December 2005; published 9 August 2006)

We computed by a Monte Carlo method, derived from the solid on solid model, the evolution during thermal treatment of a polycrystalline thin film deposited on a substrate with no further deposition. Two types of substrates have been studied: a single crystalline substrate with no defects and a single crystalline substrate with defects. We obtain islands which are either flat (i.e., with a height which does not overcome a given value) or grow in height like narrow towers. The numerical results have been qualitatively compared with experimental data: the fragmentation after thermal treatment of an yttria stabilized zirconia thin film deposited on an Al_2O_3 substrate. A good agreement was found regarding the morphology of simulated and experimental nanoislands.

DOI: 10.1103/PhysRevB.74.075411 PACS number(s): 87.53.Wz, 68.55.Jk, 68.60.Dv

I. INTRODUCTION

In recent years, the formation of mesoscopic structures on crystal surfaces has become a subject of intense experimental and theoretical study. Generally, for nonperiodically ordered nanostructures, the increasing specific area is favorable in order to enhance the physical properties (in optics, semiconducting, etc.) owing to the increased number of active sites.[1]

We will study here the evolution of a thin film deposited on a single crystalline substrate with or without defects. The thin film itself is polycrystalline with the size of crystals corresponding to the thin-film thickness. The experimental method employed to obtain such thin films is sol-gel processing.[2] The sol-gel method proceeds as follows: a thin film is deposited on a substrate by dip coating at room temperature. After a first heat treatment (stage I), the thin film of nanometric thickness is made of a large amount of nanocrystals of random orientation. At this stage the film thickness is much larger than the mean size of these nanocrystals. After a second heat treatment at higher temperature (stage II), thermal annealing induces grain growth. At this stage, the size of the crystals is of the order of the film thickness. Simultaneously, the film is submitted to fragmentation into more or less interconnected islands in order to reduce the total energy and hence reaching a more stable state.[3]

The aim of this paper is to model the spontaneous formation of nanoislands, without matter deposition, during thermal annealing of polycrystalline nanometric thin films. Much literature covers models describing the origin of islanding in homoepitaxial or heteroepitaxial single crystalline thin films.[4–10] However, models exist on nanoislands which form spontaneously without deposition.[6,11–13] In this last case, surface roughening caused by the intrinsic elastic strain and lattice mismatch between the thin film and the substrate has been experimentally studied.[14,15] Theoretical studies showed that due to morphological variations in the shape of the surface an originally flat surface of a stressed solid thin film is unstable.[16,17] Experiments showed that film roughening under various conditions and surface morphology form islands,[14,18–20] undulating surfaces,[14,21,22] and cusped surfaces.[23] Numerical models which take into account the polycrystalline character of materials can be found in Refs. 12, 13, and 24–26.

Here, we used a Monte Carlo method applied to a noncontinuous representation of a polycrystalline thin film. This model is derived from the solid on solid model but is applied here in the absence of deposition. Our model is also derived from the two-dimensional models of polycrystalline materials which computed the evolution of polycrystalline domains during thermal treatments.[28–30] Our model is based on energetic considerations: we compute the energies resulting from the elastic strains due to surface morphology of the thin film, the lattice mismatches, and the grain boundary energies. We will see that the resulting shapes of the islands depend on the relative values of these three energies. This model seems to be a good approach to describe the fundamental mechanisms of the formation of nanoislands, without matter deposition, from the breaking of a thin film under thermal annealing.

In Sec. II, we will present the model. In Sec. III, numerical results are discussed using an example of experimental result: an yttria stabilized zirconia (YSZ) thin film deposited on a Al_2O_3 substrate. Section IV corresponds to the conclusion.

II. NUMERICAL PROCEDURE

We modelled a polycrystalline thin film deposited on a single crystalline substrate either perfect or with a random distribution of defects.

Our model represents a thin film of 1 nm thickness. Each domain contains approximately 500–1000 atoms.

In the case of a substrate with no defects, the domains have a square horizontal section. The thin film is then represented by a square lattice of domains with periodic boundary conditions. This model represents a polycrystalline thin film deposited on a single crystalline substrate with no defects.

In the case of a substrate with a random distribution of defects, the sections of the domains depend on the distribution of defects. The locations of the defects are generated by a random distribution of points on the substrate. Therefore the thin film is divided into domains which correspond to the Voronoi array of the locations of the defects. The locations of

the domains do not change during computation: no displacements of the defects are occurring in the substrate. This model represents a polycrystalline thin film deposited on a single crystalline substrate with defects such as dislocations, disinclinations, and planar defects.

The mechanism of mass transport during thermal annealing is surface diffusion:

$$[J(s+ds)-J(s)]\Omega dt = \partial z \partial s, \tag{1}$$

where $J(s+ds)-J(s)$ is the transported number of atoms per unit time dt and ∂z is the height difference in thin film thickness, for change in the surface ∂s occurring during the mass transport of volume Ω.[27] The flux J may be also written:[27]

$$J = -\frac{D_s \gamma_s \Omega^{1/3}}{k_B T} \nabla k, \tag{2}$$

where k is the surface curvature, D_s is the surface diffusion constant, γ_s is the surface tension, Ω is the characteristic volume entering surface diffusion, k_B is the Boltzmann constant, and T is the absolute temperature. In terms of the characteristic measures in the system we obtain

$$J = -\frac{D_s \gamma_s \ell}{k_B T}\frac{1}{\Delta h} = \frac{D_s \gamma_s \ell}{\Delta h k_B T}, \tag{3}$$

where $\ell \propto \Omega^{1/3}$ is the characteristic mean size of the domains and Δh is the difference of heights for two locations at a distance ℓ. Similarly, in terms of characteristic measures, Eq. (1) yields

$$J = -\frac{\Delta h}{\ell \Delta t} \tag{4}$$

for one time interval Δt and for $s \propto \ell^2$. Finally, relating Eqs. (3) and (4) holds:

$$\Delta h = \sqrt{\frac{\ell^2 D_s \gamma_s \Delta t}{k_B T}}. \tag{5}$$

Hence if we assume that the stress tensor inside the thin film is diagonal (for example, for cubic phase thin films) the energy related to Δh using the work of elastic forces, the Young modulus Y, and the Poisson ratio ν is

$$\begin{aligned} E_h &= Y(1+\nu)\Delta h \ell [h(t+\Delta t)-h(t)] \\ &= Y(1+\nu)\ell^2 \sqrt{\frac{D_s \gamma_s \Delta t}{k_B T}}[h(t+\Delta t)-h(t)], \end{aligned} \tag{6}$$

where $[h(t+\Delta t)-h(t)]$ is the displacement in the normal direction of the thin film for a time interval Δt and ℓ is the displacement in horizontal direction related to the Poisson ratio ν.

If we deal with crystallographic orientations, let us report the behavior of single crystalline grain growth[28] where the driving force for change in the crystallographic orientation is related to the difference in pressure:

$$\Delta p_{ij} = 2\gamma_b \left(\frac{1}{R_i} - \frac{1}{R_j}\right), \tag{7}$$

where R_i is the sphere equivalent radius of the domain i, γ_b is grain boundary surface tension, and p_{ij} is the pressure. Several domains with the same crystallographic orientation may form the same grain. Hence the growth of one grain is equivalent to the changes in crystallographic orientation of its neighboring domains. If we use the characteristic measures of the system, with Eq. (7), we obtain the energy necessary to change the crystallographic orientation of one domain by calculating the work of the driving force deduced from the pressure:

$$\begin{aligned} E_b &= \gamma_b \ell^2 \left(\frac{1}{h} + \frac{1}{\ell}\right)[s(t+\Delta t)-s(t)] \\ &= \gamma_b \left(\frac{\ell^2}{h} + \ell\right)[s(t+\Delta t)-s(t)], \end{aligned} \tag{8}$$

where $[s(t+\Delta t)-s(t)]$, associated to the work of the driving force given by Eq. (7) has the dimension of a length. The parameter s is the interplane spacing of the family planes which corresponds to one of the vertical domain-domain interfaces or to the horizontal domain-substrate interface of an elementary domain. Thus the value of s is defined as $s = 1/|\vec{r}|$, where $\vec{r}$ (the reciprocal-space lattice vector in m^{-1}) is orthogonal to the family planes. Therefore the crystallographic reorientation of a domain may be related to the modification of the interplane spacing as given in Eq. (8).

Straightforwardly, we consider here three aspects which contribute to the energy of our thin film consisting of crystal species: the grain-boundary energy (which here is equivalent to the interfacial energy between two elementary domains of different crystallographic orientations), the interfacial energy (which corresponds to the difference of energy between one elementary domain and the substrate), and the surface energy (which is related here to the height of each elementary domain). For our system of N lattice domains, the energy necessary to change crystallographic orientation and height for domain i with respect to domain j becomes

$$\begin{aligned} E_i = {} & B\left(\frac{\ell_i^2}{h_i} + \ell_i\right)\sum_{j=1}^{NN}[c_i - c_s - (c_j - c_s)] \\ & + C\left(\frac{\ell_i^2}{h_i} + \ell_i\right)\sum_{j=1}^{NN}[d_i - d_s - (d_j - d_s)] + D\ell_i^2 \sum_{j=1}^{NN}(h_i - h_j), \end{aligned} \tag{9}$$

where h_i is the height of elementary domain i, c_i and c_j are the interplanes spacings of the family planes of the domains i and j in the horizontal plane (parallel to the surface of the substrate), and c_s is the interplane spacing of the family planes of the substrate in the same plane. The length c_s is constant. The parameters d_i and d_j are the interplane spacings of the family planes in the vertical plane (orthogonal to the substrate's surface) of domains i and j. Finally, d_s is the interplane spacing of the family planes of the substrate in the same plane. The previous equality may be simplified as

$$E_i = B\left(\frac{\ell_i^2}{h_i} + \ell_i\right)\sum_{j=1}^{NN}(c_i - c_j) + C\left(\frac{\ell_i^2}{h_i} + \ell_i\right)\sum_{j=1}^{NN}(d_i - d_j) + D\ell_i^2\sum_{j=1}^{NN}(h_i - h_j). \quad (10)$$

The first and second terms of the right-hand side of the equality correspond to the interfacial energy coming from the energy with respect to the substrate and from the grain-boundary energy. The third term corresponds to the surface energy related to the heights of the domains [see Eq. (6)]. NN is the nearest-neighbors number of a lattice domain. $B = \gamma_{b1}$ scales the interfacial energy between two elementary domains and is the boundary surface tension. $C = \gamma_{b2}$ scales the interfacial energy with respect to the substrate where γ_{b2} is the interfacial surface tension of the domains with respect to the substrate. D scales the surface strain obtained for different heights of the elementary domains:

$$D = Y(1+\nu)\sqrt{\frac{D_s\gamma_s\Delta t}{k_B T}}. \quad (11)$$

The values of c and d range from the upper value of the interplane spacing in horizontal and vertical planes, respectively, and have the dimension of a length. The time interval Δt is chosen to be constant.

For Monte Carlo simulations of single phase films, only one type of event, namely lattice domain reorientation, was considered.[28–30] In our model, the height of each elementary domain is also submitted to change as in the SOS model. But, unlike traditional SOS models, a species at domain i may change its orientation with respect to its nearest-neighbor and to the substrate.

In our model, each domain owns three states (c,d,h). h has its value ranging from 0 nm to a value that depends on the physical properties of the thin film as will be seen in the results.

At the begining of computation, i.e., at $t=0$ Monte Carlo steps (MCS) all elementary domains were assumed to have a height of 1 nm and a random crystallographic orientation. After such initialization, the Monte Carlo algorithm works according to the classical Metropolis scheme.[31] A lattice domain is chosen at random for three events (changes in the projections of the crystallographic orientation and height exchange) occurring. A neighbor of this domain is also chosen at random, and the energy given by Eq. (10) is computed.

The probability for each event is given by P in which $\Delta E = E_1 - E_2$, where E_1 and E_2 are energies given by Eq. (10), of the present configuration and the configuration which the system may reach, respectively,

$$P = 1 \quad \text{if } \Delta E <= 0, \quad (12)$$

$$P = \exp\left(\frac{-\Delta E}{k_B T}\right) \quad \text{if } \Delta E > 0, \quad (13)$$

where k_B is the Boltzmann constant and T is the simulation temperature. Note that, as height exchange and crystallographic reorientation are not independent events, it may occur that a domain changes its height inducing a change in the orientational energy of the domain. Moreover, we used a Monte Carlo technique to study the statistical sampling of the thin-film geometry, due to its surface topology. The values of B, C, and D may vary as well as the absolute temperature T. Note that in the following we will call c_s and d_s either crystallographic orientations or interplanes spacings.

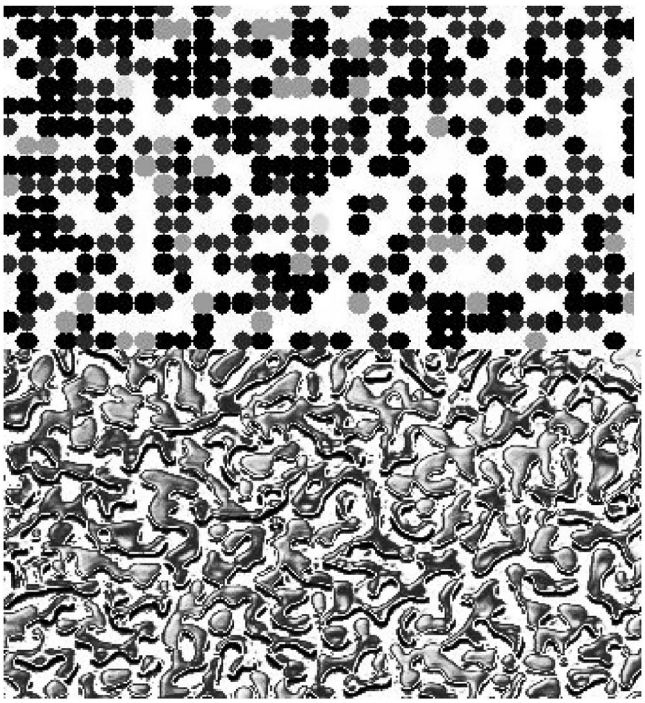

FIG. 1. Top: Fragmentation of a simulated thin film with a square array of domains. The color of the circles ranges from black domains of height $h=1$ nm to light domains of larger heights of the corresponding domain. Bottom: Electronic microscope image of a zirconia fragmented experimental thin film, light zones correspond to larger thickness of the fragmented thin film.

III. RESULTS AND DISCUSSION

We computed all the results presented in the following figures at a temperature $T=1800$ K which corresponds to experimental data (see below). The typical size of an interplane spacing in a crystalline lattice is 2 Å which corresponds to ten atoms. An elementary domain of the simulated thin film is composed of 1000 atoms, which implies an average interplane spacing around 20 Å or 2 nm. Consequently, the values of 0.5 and d may be enclosed between 0.5 and 2.5 nm. At $t=0$ MCS the simulated thin film is perfectly flat and is $h=1$ nm thick, i.e., all domains have the same height $h=1$ nm. Numerical results have been averaged over five runs. All the thin films are represented by a square of edge equal to 100 nm divided in 10 000 domains with periodic boundary conditions. For the square lattice, each domain is 1 nm wide. For the random array, the domains are randomly distributed.

In Fig. 1, top image, one can see the resulting fragmentation of a thin film deposited on a square lattice. This figure is obtained after $t=10^9$ MCS. The image in the bottom of Fig.

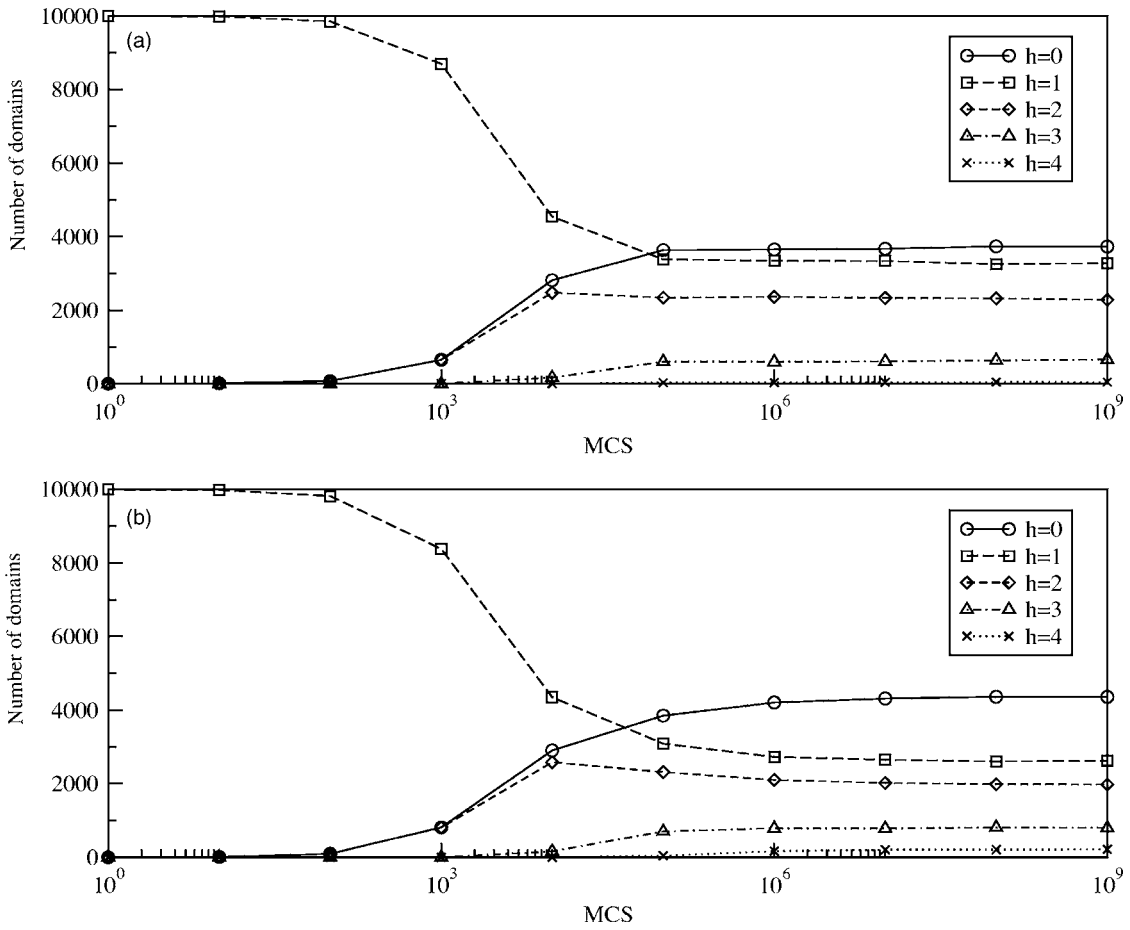

FIG. 2. (a) Evolution of the number of domains with heights $h=0,1,2,3,4$ nm as a function of MCS for a square array of domains corresponding to a substrate with no defects. (b) Evolution of the number of domains with heights $h=0,1,2,3,4$ nm as a function of MCS for a random array of domains corresponding to a substrate with defects. The parameters for (a) and (b) are $B=1$ J m^{-2}, $C=1$ J m^{-2}, and $D=1$ J m^{-3}.

1 corresponds to a YSZ thin film after thermal annealing at 1500 °C. This experimental thin film has been deposited by a sol-gel process (introduced in Sec. I) on a perfect single crystalline substrate of Al_2O_3. Good qualitative agreement is found regarding the dewetting and the morphology of the fragmented thin film, for simulated and experimental thin film. The differences come from the facts that the simulated thin film is on lattice and that the domains have been represented by circles.

A. Crystallographic orientations and heights of the domains

The aim of this section is to understand the influence of the substrate on the evolution of the heights and crystallographic orientations of the elementary domains. Consequently B, C, and D are arbitrarily chosen to be equal and constant. We performed the Monte Carlo process as written in Sec. II, for the two kinds of substrate, i.e., with or without defects. In Fig. 2(a), the evolution of the heights of the domains can be seen as a function of MCS, for $B=1$ J m^{-2}, $C=1$ J m^{-2}, and $D=1$ J m^{-3}, in the case of a periodic (square) array of domains. Figure 2(b) corresponds to the same evolution with the same numerical values of B, C, and D but for a random array of domains. One may see in these two figures that the number of domains with heights $h=0$ nm increases until equilibrium is reached. During the same time, the number of domains with heights $h=2$, 3, and 4 nm increases while the number of domains with heights $h=4$ nm decreases until reaching equilibrium at $t=10^5$ MCS. There is a difference between the two figures regarding the number of domains with height $h=0$ nm: for a periodic array of domains this number is lower than for a random array of domains. This allows us to say that defects on the substrate lead to a larger dewetting of the thin film. We will see below that, depending on the relative values of B, C, and D this dewetting may vary.

Figures 3(a) and 3(b) show the evolution of the orientations c and d as a function of MCS, for $B=1$ J m^{-2}, $C=1$ J m^{-2}, and $D=1$ J m^{-3}, in the case of a periodic (square) array of domains, where c and d vary from 0.5 to 2.5 nm. Figures 3(c) and 3(d) correspond to the evolution of the orientations c and d as a function of MCS, for $B=1$ J m^{-2}, $C=1$ J m^{-2}, and $D=1$ J m^{-3}, in the case of a random array of domains and for the same range of c and d. In Figs. 3(a) and 3(b), we see that all domains (for a periodic array of domains) change from a random distribution of crystallographic orientations to a heteroepitaxial crystallographic ori-

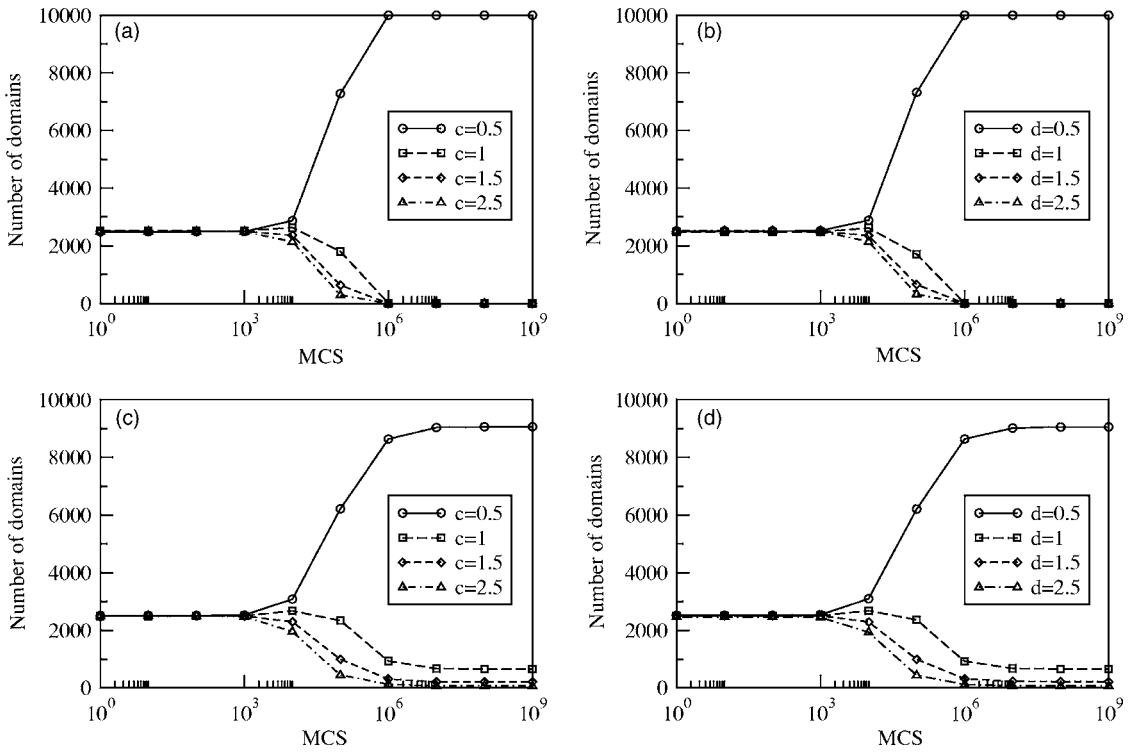

FIG. 3. (a) Evolution of the vertical crystallographic orientation $c=0.5,1,1.5,2.5$ nm as a function of MCS for a substrate with no defects. (b) Evolution of the horizontal crystallographic orientation $d=0.5,1,1.5,2.5$ nm as a function of MCS for a substrate with no defects. (c) Evolution of the vertical crystallographic orientation $c=0.5,1,1.5,2.5$ nm as a function of MCS for a substrate with defects. (d) Evolution of the horizontal crystallographic orientation $d=0.5,1,1.5,2.5$ nm as a function of MCS for a substrate with defects. The parameters for this figure are $B=1$ J m^{-2}, $C=1$ J m^{-2}, and $D=1$ J m^{-3}.

entation. Indeed, all domains for the two types of substrates get the lowest crystallographic orientation regarding its energy for $t=10^6$ MCS. In Figs. 3(c) and 3(d) we see that not all domains have reached the lowest crystallographic orientation with respect to their energy when there are defects on the substrate (random array of domains).

B. Influence of factors *B*, *C*, and *D*

In this section, we study the evolution of the heights and crystallographic orientations of the domains as a function of MCS. As in the previous part, the parameters B, C, and D are chosen arbitrarily but their relative values are deeply different in order to highlight their effects on the heights and crystallographic orientations of the domains.

In Fig. 4 the evolution of the crystallographic orientations c and d are plotted as a function of MCS for $B=10^{-5}$ J m^{-2}, $C=1$ J m^{-2}, and $D=1$ J m^{-3} for a square array of domains (respectively for a random array of domains). This figure corresponds to an average over five runs. The evolution of c is clearly different for these values of B, C, and D from the results obtained in Fig. 3, for a square array of domains as well as for a random array of domains.

Let us analyze Fig. 4. In this case, $B=10^{-5}$ J m^{-2} while $C=1$ J m^{-2} and $D=1$ J m^{-3}. The horizontal crystallographic orientations depend on the initial configuration of the different horizontal crystallographic orientations. As $B=10^{-5}$ J m^{-2} is very low, it induces a low energy corresponding to the crystallographic orientation. So depending on the relative numbers of the different values of c_i and as the value of the probability of c_i values exchanges is close to 1 for each MCS, the resulting behavior of the number of relative values of c_i follows a random behavior. Equilibrium has not been reached in this case and the respective numbers of the different values of c may change even after $t=10^9$ MCS. We checked this by making other runs of our program, and the resulting evolution of c was different for different averages. We obtained a textured thin film.

We may say that the influence of the value of the constant C is the same as that of constant B as these two constants are symmetrical and may be exchanged in Eq. (10).

In Fig. 5 the evolution of the heights as a function of MCS is shown for $B=10^5$ J m^{-2}, $C=10^5$ J m^{-2}, and $D=10^{-5}$ J m^{-3} for a square array of domains [Fig. 5(a) and 5(b)] and for a random array of domains [Figs. 5(c) and 5(d)]. Figure 5 shows the evolution of the number of domains with heights ranging from $h=0$ nm to $h=10$ nm for the two kinds of substrates. The evolution of the number of domains with heights ranging from $h=0$ nm to $h=4$ nm shows that dewetting is larger and faster. The numbers of domains of heights ranging from $h=5$ nm to $h=10$ nm increase until reaching an equilibrium for $t=10^9$ MCS.

In the case of Fig. 5(a) corresponding to the values $B=C=10^5$ J m^{-2} and $D=10^{-5}$ J m^{-3}, the evolution of the number of domains with heights $h=0,1,2,3,4$ nm for the square lattice of domains follows the same typical behavior as for the case where $B=C=1$ J m^{-2} and $D=1$ J m^{-3} but with a

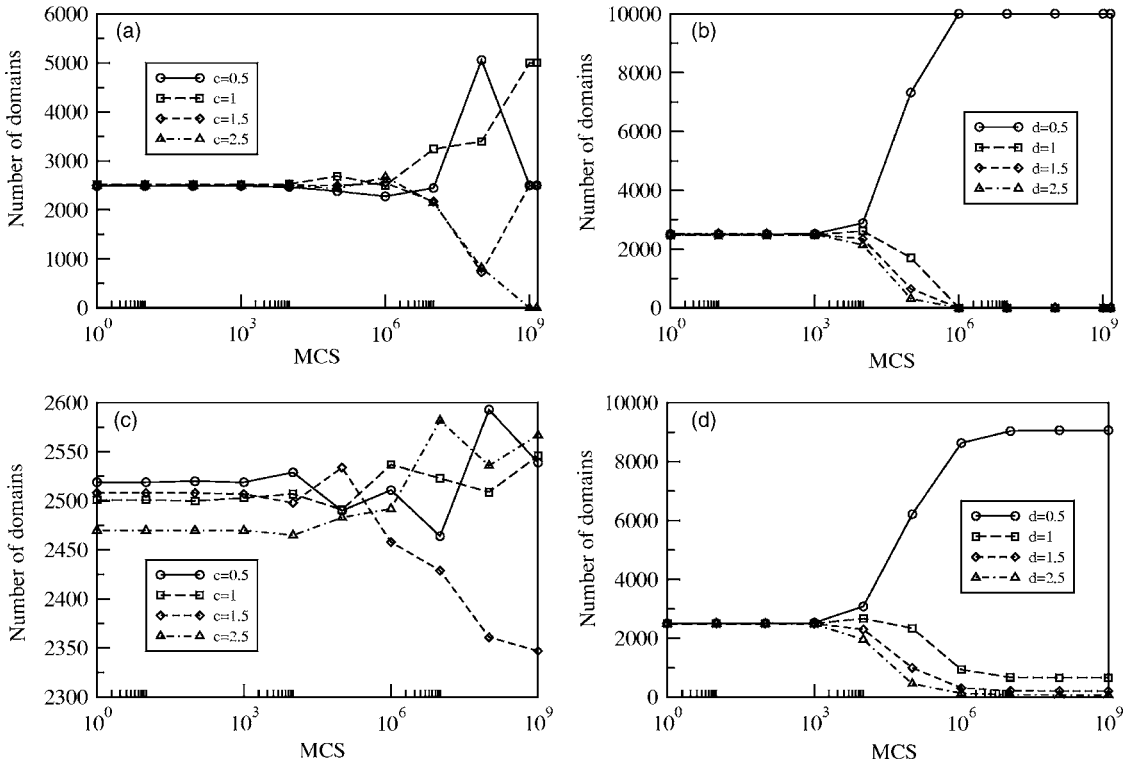

FIG. 4. (a) Evolution of the vertical crystallographic orientation $c=0.5,1,1.5,2.5$ nm as a function of MCS for a substrate with no defects. (b) Evolution of the horizontal crystallographic orientation $d=0.5,1,1.5,2.5$ nm as a function of MCS for a substrate with no defects. (c) Evolution of the vertical crystallographic orientation $c=0.5,1,1.5,2.5$ nm as a function of MCS for a substrate with defects. (d) Evolution of the horizontal crystallographic orientation $d=0.5,1,1.5,2.5$ nm as a function of MCS for a substrate with defects. The parameters for this figure are $B=10^{-5}$ J m^{-2}, $C=1$ J m^{-2}, and $D=1$ J m^{-3}.

faster dewetting. Figures 5(b) and 5(d) show the appearance of domains with heights larger than 4 nm. In the case of the random array of domains, the dewetting process is strong at $t=10^9$ MCS. Moreover, one can observe in Figs. 5(b) and 5(d) that the numbers of domains with heights $h=5,6,7,8$ nm is not negligible. These preceding numbers reach an equilibrium after $t=10^9$ MCS. In the case of Fig. 5(d), there are more domains which grow in height for a substrate with defects compared to the perfect substrate giving the results of Fig. 5(b).

C. Substrate with defects: Comparison with experiments

The previous sections (Secs. III A and III B) demonstrated the effects of defects on the evolution of the domains. A random array of domains leads to a higher dewetting of the substrate due to the relaxation of the stresses imposed by the defects at the film-substrate interface. The aim of this part is to qualitatively compare the experimental and simulated thin film after thermal treatment. We describe now an experimental procedure to synthesize an yttria stabilized zirconia (YSZ) thin film deposited on an Al_2O_3 substrate with defects. (YSZ) thin films were elaborated by sol-gel dip coating.[15] First of all, clear homogeneous sols were prepared from zirconium *n*-propoxide, acetylacetone, and *n*-propanol. Yttrium nitrate $[Y(NO_3)_3(H_2O)_5]$ dissolved in *n*-propanol was used as the Y_2O_3 precursor. The yttria content was set to 10 mol so that YSZ is expected to crystallize in its cubic phase. A *c*-cut sapphire substrate was roughly polished in order to create defects. The roughly mechanical-chemical polishing was realized with colloidal silica dispersed into an acid solution. A short thermal treatment at high temperature (set to 15 min at 1500 °C) was necessary to get rid of high residual polishing-induced strains and to perform a very small mosaicity allowing the epitaxy of the thin film. A continuous amorphous film is realized by dip coating after the setting of the zirconium *n*-propoxide concentration into the precursor solution equal to $[Zr]=0.025$ mol l^{-1}. The dipping speed was fixed to 1.67 mm s^{-1}. These parameters allow us to control the thickness of the continuous films which is close to 5 nm in that case. A small thickness was chosen in order to maximize the interfacial effects. A primary thermal treatment at 600 °C induces the crystallization of the films which is made of randomly oriented nanocrystals of zirconia. Another thermal treatment at higher temperature (15 min at 1500 °C) induces the breaking up of the film and the formation of epitaxial YSZ islands. YSZ is in the cubic phase. In order to compare the numerical results with the experimental ones, the parameters used in the model have been calculated from data in literature: $Y=300$ GPa, $\nu=0.3$, $\ell=1$ nm, $D_s=8\times10^{-5}$ m^2 s^{-1},[32] $\gamma_s=620\times10^{-3}$ J m^{-2},[33] Δt is of the order of 10^4 s and $k_BT=2$ J. Thus the parameter D has been calculated using Eq. (11). We can consider that, as YSZ is in its cubic phase, the value of parameter γ_s does not change with crystallographic orientation due to quasi-isotropy. For example, the data in literature give an error of 20% on the

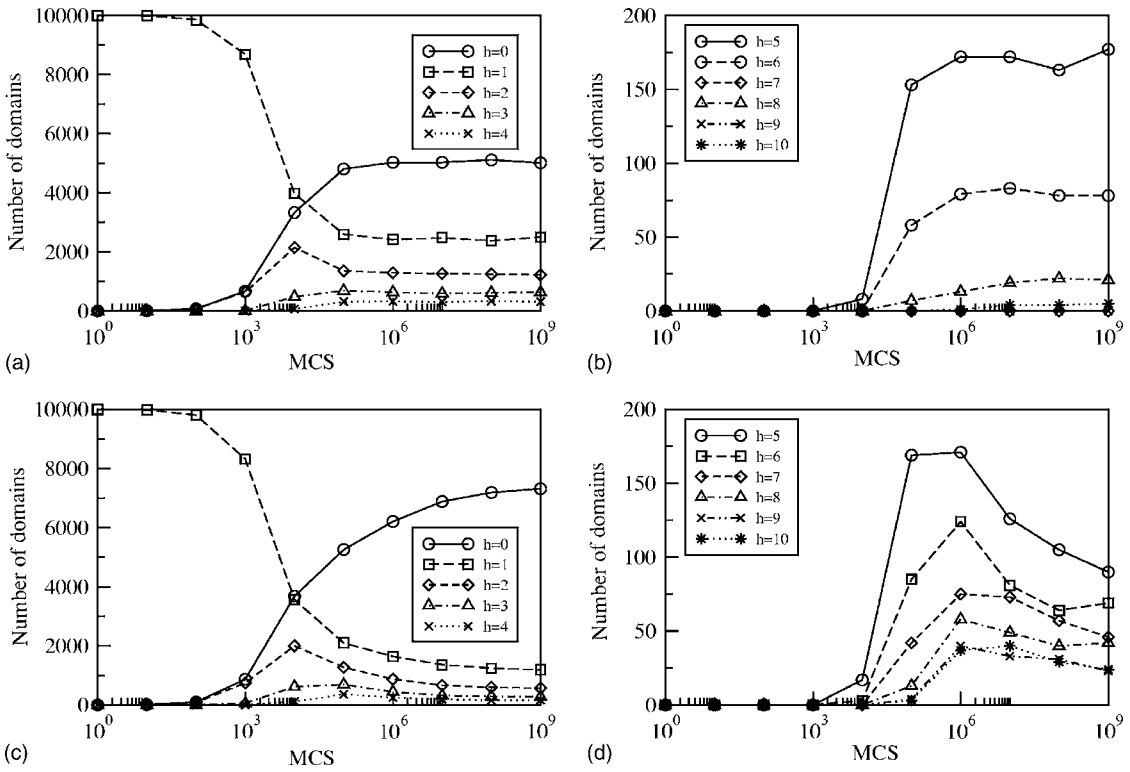

FIG. 5. (a) Evolution of the number of domains with heights $h=0,1,2,3,4$ nm as a function of MCS for a square array of domains corresponding to a substrate with no defects. (b) Evolution of the number of domains with heights $h=5,6,7,8,9,10$ nm as a function of MCS for a square array of domains corresponding to a substrate with no defects. (c) Evolution of the number of domains with heights $h=0,1,2,3,4$ nm as a function of MCS for a random array of domains corresponding to a substrate with defects. (d) Evolution of the number of domains with heights $h=5,6,7,8,9,10$ nm as a function of MCS for a random array of domains corresponding to a substrate with defects. The parameters for (d) are $B=10^5$ J m^{-2}, $C=10^5$ J m^{-2}, and $D=10^{-5}$ J m^{-3}.

value of γ_s for all orientations.[33] Therefore the values of γ_{b1} and γ_{b2} are of the same order as γ_s and $B= C=\gamma_s$.

We compared a top view of an experimental thin film with a top view of a simulated thin film. Figure 6 is the top view of an experimental YSZ thin film on a *c*-cut saphire substrate with defects. These experimental defects have been obtained by rough mechanical-chemical polishing. Figure 7 is a top view of a fragmented simulated thin film on a substrate with defects for the numerical values of B, C, D corresponding to the experimental parameters. The dark disks correspond to islands of 1 nm height, the other disks correspond to higher islands which are as clear as they are high. The difference between the lateral size of the sample and distances between high domains comes from the fact that the duration of experimental thermal treatment cannot be simulated in a reasonable computing time.

D. Discussion

In the case of a substrate without defects, the dewetting observed for a simulated thin films (square lattice) is in good agreement with the experimental results concerning YSZ thin film deposited on a Al_2O_3 *c*-cut substrate (see Fig. 1, top for simulation and bottom for experiment). In the case of a substrate with defects, results from simulated and experimental thin film after islanding are also in good qualitative agreement (see Figs. 6 and 7). The numerical model allows one to say that the defects are responsible for the stronger dewetting occurring in this situation. The physical interpretation of this result was introduced in a previous paper concerning the

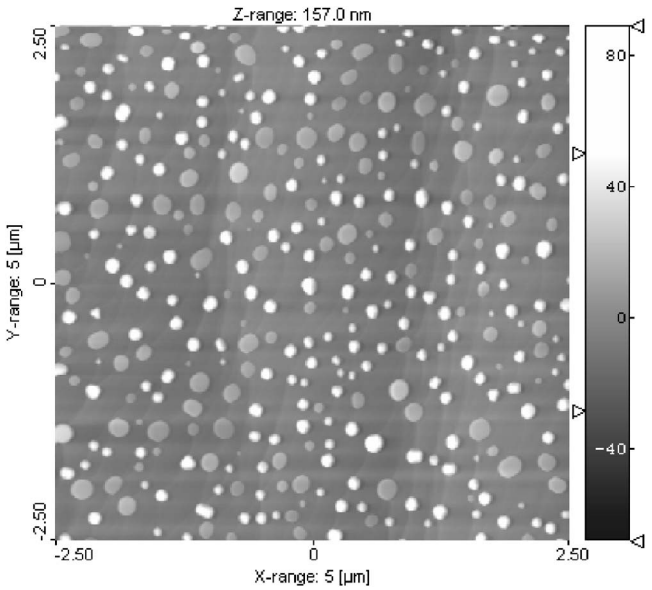

FIG. 6. AFM topography of a YSZ thin-film island on a substrate with defects; the greyscale on the right determines the height of the nanoislands.

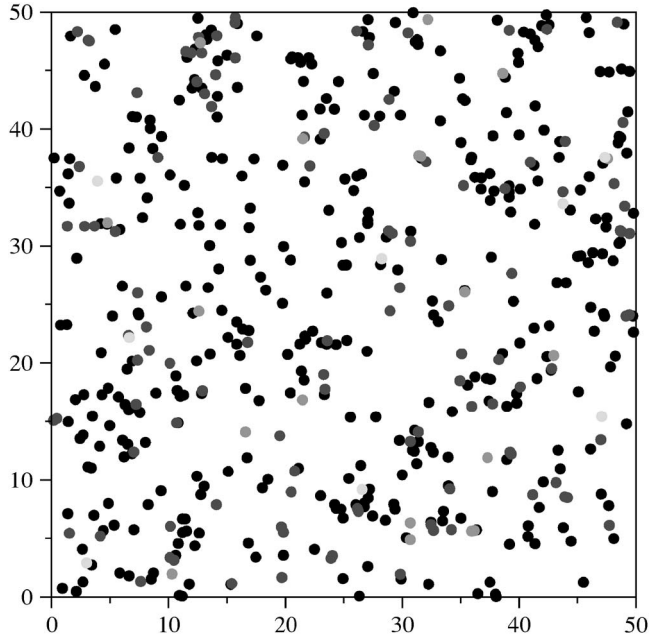

FIG. 7. Simulated image of islands corresponding to experimental values of parameters B, C, and D. Islands of height $h=1$ nm are in black and islands of larger heights have a color which gets lighter as a function of height.

dewetting of thin films on quasicrystalline substrate (the thin film was modeled with elementary domains surrounded by five, six, or seven neighbors).[12] The authors demonstrated that "the influence of the geometry of the substrate" (i.e., the surfacic concentration of defects) "leads to an intrinsic stress inside the film." In other words, the domains of the numerical thin film surrounded by the more numerous neighbors were submitted to higher stresses than the ones with fewer neighbors; thus the film broke into islands, through the height increase of the domains proportionally to the intensity of the local stress concentrations. We can assume that this interpretation is still relevant for a substrate with defects randomly distributed. Therefore such a substrate applies stresses inside the thin film and nanoislands grow in height at the locations of the maximum concentrations of defects.

IV. CONCLUSION

We modeled the islanding, without deposition, of polycrystalline thin films by a Monte Carlo process taking into account the crystallographic orientations of the grains and the heights of each nanometric domain composing the underlying lattice representing the thin film. The governing equation allowing us to compute the energy of each of these domains takes into account the surface tension on surfaces, the grain-boundaries energies, the surface diffusion constant, and the elasticity of the thin film. Depending on the values of these parameters, we obtain different evolutions of the distribution of crystallographic orientations and of the dewetting. The dewetting is larger for substrates with defects. This characteristic is also obtained in experimental thin films after thermal annealing. Straightforwardly, for substrates with defects, experiments and numerical simulations show a higher increaser in height of the islands than is the case on perfectly single crystalline substrates.

[1] V. M. Shalaev, *Optical Properties of Nanostructured Media*, Springer Topics in Applied Physics, Vol. 82 (Springer, New York, 2002).
[2] J. F. Brinker and G. W. Scherer, *Sol Gel Science: The Physics and Chemistry of Sol Gel Processing* (Academic, New York, 1990).
[3] K. T. Miller, F. F. Lange, and D. B. Marshall, J. Mater. Res. **5**, 151 (1990).
[4] V. A. Shchukin and D. Bimberg, Rev. Mod. Phys. **71**, 1125 (1999).
[5] A. A. Golovin, S. H. Davis, and P. W. Voorhees, Phys. Rev. E **68**, 056203 (2003).
[6] W. T. Tekalign and B. J. Spencer, J. Appl. Phys. **96**, 5505 (2004).
[7] B. J. Spencer, P. W. Voorhees, and S. H. Davis, Phys. Rev. Lett. **67**, 3696 (1991).
[8] B. J. Spencer, Phys. Rev. B **59**, 2011 (1999).
[9] H. R. Eisenberg and D. Kandel, Phys. Rev. B **66**, 155429 (2002).
[10] Y. W. Zhang, Phys. Rev. B **61**, 10388 (2000).
[11] Y. W. Zhang, Thin Solid Films **357**, 8 (1999).
[12] N. Olivi-Tran, A. Boulle, A. Gaudon, and A. Dauger, Phys. Lett. A (to be published).
[13] X. Zhou, N. Olivi-Tran, A. Gaudon, and A. Dauger, J. Alloys Compd. (to be published).
[14] B. Wang, Y. Peng, F. Zhao, W. Chen, S. Liu, and C. Gao, J. Cryst. Growth **186**, 43 (1998).
[15] R. Bachelet, A. Boulle, B. Soulestin, F. Rossignol, A. Dauger, and R. Guinebretiere (unpublished).
[16] B. J. Spencer, P. W. Voorhees, and S. H. Davis, J. Appl. Phys. **73**, 4955 (1993).
[17] L. B. Freund and F. Jonsdottir, J. Mech. Phys. Solids **41**, 1245 (1993).
[18] D. J. Eaglesham and M. Cerullo, Phys. Rev. Lett. **64**, 1943 (1990).
[19] C. W. Snyder, B. G. Orr, D. Kessler, and L. M. Sander, Phys. Rev. Lett. **66**, 3032 (1991).
[20] J. Tersoff and F. K. LeGoues, Phys. Rev. Lett. **72**, 3570 (1994).
[21] J. Y. Yao, T. G. Anderson, and G. L. Dunlop, Appl. Phys. Lett. **53**, 1420 (1988).
[22] A. J. Pidduck, D. J. Robbins, A. G. Cullis, W. Y. Leong, and A. M. Pitt, Thin Solid Films **222**, 78 (1992).
[23] D. E. Jesson, S. J. Pennycook, J. M. Baribeau, and D. C. Houghton, Phys. Rev. Lett. **71**, 1744 (1993).
[24] M. E. Glicksman, J. Mater. Sci. **40**, 2149 (2005), and references within.
[25] B. Sun, Z. Suo, and W. Yang, Acta Mater. **45**, 1907 (1997), and references within.
[26] B. Sun and Z. Suo, Acta Mater. **45**, 4953 (1997), and references within.
[27] R. Thouy, N. Olivi-Tran, and R. Jullien, Phys. Rev. B **56**, 5321

(1997).
[28] M. P. Anderson, D. J. Srolovitz, G. S. Grest, and P. S. Sahni, Acta Metall. **32**, 783 (1984).
[29] D. J. Srolovitz, J. Vac. Sci. Technol. A **4**, 2925 (1986).
[30] D. J. Srolovitz, A. Mazor, and B. G. Bukiet, J. Vac. Sci. Technol. A **6**, 237L (1986).
[31] N. Metropolis, A. W. Rosenbluth, M. N. Rosenbluth, A. T. Teller, and E. J. Teller, Chem. Phys. **21**, 1087 (1953).
[32] M. de Ridder, R. G. van Welzenis, H. H. Brongersma, and V. Kreissig, Solid State Ionics **158**, 67 (2003).
[33] P. Pascal, *Nouveau Traité de Chimie Minérale, Tome IX, Titane, Zirconium, Hafnium, Thorium* (Masson Eds., Paris, 1963).